The International Journal of Engineering and Science (IJES)
ISSN (e): 2319 – 1813 ISSN (p): 23-19 – 1805
|| Pages || PP 58-64 || 2020 ||

Numerical investigation of natural convection of AL_2O_3 - water nanofluid in an openended square cavity heated sinusoidally

Prabir Barman[1], Pentyala Srinivasa Rao[1]
[1]*Department of Mathematics and Computing, IIT(ISM) Dhanbad, Jharkhand, India*
Corresponding Author: Pentyala Srinivasa Rao

----------***ABSTRACT***----------
In this article, natural convection of AL_2O_3-water nanofluid in an open cavity under the presence of sinusoidal heating is investigated numerically. The cavity is placed horizontal and right end is open to cold nanofluid and left vertical wall is heated keeping top and bottom as adiabatic. From the open end of the cavity cold AL_2O_3-water nanofluid is injected. The flow inside the cavity is due to density variation caused by temperature difference (buoyancy force).The non-dimensional governing equations are solved by finite difference method. The main parameters involving the investigation are Rayleigh number$(10^4 \leq Ra \leq 10^5)$, nanoparticles volume friction$(0.0 \leq \phi \leq 0.04)$ and phase shift of the heating temperature$(0 \leq \gamma \leq \pi)$. It is observed that sinusoidal heating changed direction of heat flow (environment to cavity and cavity to environment), phase change changes the position of heat transfer direction. The presence of nanoparticles under sinusoidal heating enhances heat propagation and as Ra increases, heat propagation decreases.
KEYWORDS; -*partially open cavity, Sinusoidal heating, Nanofluid, Natural convection*

I. INTRODUCTION

Natural convection in an open-ended cavity is an area of great interest, lot of work has been done in the context of natural convection in an open ended cavity. Studies such as, Ostrach [1], Bilgen et al. [2], Öztop et al. [3] considered comprehensive review of convection in an enclosure with heat heating on one side having uniform heating profile. But in most realistic cases, the heating may be on either side having sinusoidal kind of profile rather than uniform profile. Also, the study of natural convection in an open ended cavity has applications in industry and in domestic equipments, a numerical study of convection in open ended cavity having two porous layers inside was studied by Miroshnichenko et al. [4].

The objective of the present work is to study natural convection inside an open-ended square cavity with sinusoidal heat profile from vertical wall the left wall of the cavity is heated sinusoidally and right end is open having top and bottom walls are adiabatic. Based on the above literature survey and authors' knowledge this proposed model on natural convection is discussed for first time. There is no work on natural convection in an open ended cavity with sinusoidal heating.

II. GOVERNING EQUATIONS

Natural convection in an open square cavity of length and height L filled with Al_2O_3- nanofluid submitted to sinusoidal heating with difference phase shift of heating temperature have been investigated. Sketch of domain of interest and coordinate system along with boundary conditions, the sinusoidal heating profile for different phases and grid distribution inside domain of computation are shown in $Fig.1$.

The cavity has been kept horizontal and bottom wall is considered as *x*-axis and left vertical wall as *y*-axis and body force, gravity, are acting vertically downwards. Aspect ratio of the cavity is considered to be unity and amplitude of the sinusoidal heating profile is considered as *0.5*. The thermophysical properties of nanofluid are taken from [4] and fluid phase, nanoparticle thermal equilibrium is considered.

The non-dimensional governing equations in stream function-vorticity $(\omega - \psi)$ formulation for flow in 2D are as follows:

$$\frac{\partial^2\psi}{\partial\bar{x}^2} + \frac{\partial^2\psi}{\partial\bar{y}^2} = -\omega \tag{1}$$

$$\bar{u}\frac{\partial\omega}{\partial\bar{x}} + \bar{v}\frac{\partial\omega}{\partial\bar{y}} = H_1(\phi)\sqrt{\frac{Pr}{Ra}}\left(\frac{\partial^2\omega}{\partial\bar{x}^2} + \frac{\partial^2\omega}{\partial\bar{y}^2}\right) + H_2(\phi)\frac{\partial\theta}{\partial\bar{x}} \tag{2}$$

$$\bar{u}\frac{\partial\theta}{\partial\bar{x}} + \bar{v}\frac{\partial\theta}{\partial\bar{y}} = \frac{H_3(\phi)}{\sqrt{Ra.Pr}}\left(\frac{\partial^2\theta}{\partial\bar{x}^2} + \frac{\partial^2\theta}{\partial\bar{y}^2}\right) \tag{3}$$

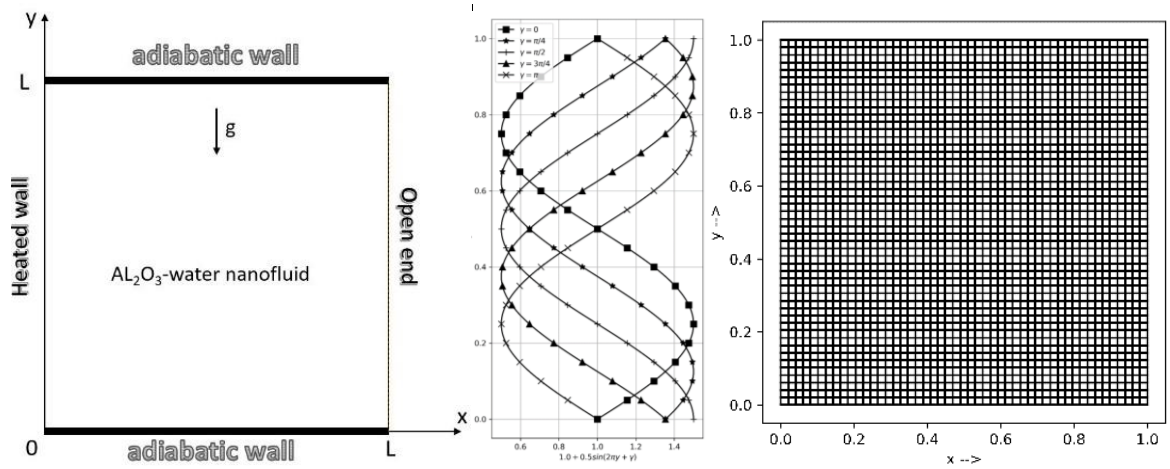

Fig. 1. left: Domain of computation and dimensional coordinates, middle: heating profile at left boundary, right: grid distribution in computational domain.

The non-dimensional boundary conditions are:

$$\psi = 0, \omega = -\frac{\partial^2 \psi}{\partial \bar{x}^2}, \theta = 1 + a\sin(2\pi\bar{x} + \gamma) \text{ at } \bar{x} = 0 \quad (4)$$

$$\frac{\partial \psi}{\partial \bar{x}} = 0, \frac{\partial \omega}{\partial \bar{x}} = 0, \begin{cases} if\ \frac{\partial \psi}{\partial \bar{y}} \geq 0, then\ \frac{\partial \theta}{\partial \bar{x}} = 0 \\ if\ \frac{\partial \psi}{\partial \bar{y}} < 0, then\ \theta = 0 \end{cases} \text{ at } \bar{x} = 1 \quad (5)$$

$$\psi = 0, \omega = -\frac{\partial^2 \psi}{\partial \bar{y}^2}, \frac{\partial \theta}{\partial \bar{y}} = 0 \text{ at } \bar{y} = 0 \text{ and at } \bar{y} = 1 \quad (6)$$

We employed $\bar{x} = x/L$, $\bar{y} = y/L$, $\bar{u} = u / \sqrt{g\beta(T_h - T_c)L}$, $\bar{v} = v / \sqrt{g\beta(T_h - T_c)L}$, $\theta = (T - T_c) / (T_h - T_c)$ variables to obtain the non-dimensional governing equations (1)-(3). Here, ψ ($\bar{u} = \partial\psi/\partial\bar{y}$, $\bar{v} = -\partial\psi/\partial\bar{x}$) is non-dimensional stream-function and $\omega = \frac{\partial \bar{v}}{\partial \bar{x}} - \frac{\partial \bar{u}}{\partial \bar{y}}$ is non-dimensional vorticity.

Here Prandtl number, $Pr = \mu_f (\rho c)_f / (\rho_f \lambda_f)$ and Rayleigh number, $Ra = g(\rho\beta)_f (\rho c)_f (T_h - T_c) L^3 / (\mu_f \lambda_f)$ are dimensionless numbers. $H_1(\phi), H_2(\phi), H_3(\phi)$ are special functions defined as,

$$H_1(\phi) = \frac{\mu_{nf}}{\mu_f}\frac{\rho_f}{\rho_{nf}} = \frac{1 + 4.93\phi + 222.4\phi^2}{1 - \phi + \phi\,\rho_p/\rho_f}$$

$$H_2(\phi) = \frac{(\rho\beta)_{nf}}{(\rho\beta)_f}\frac{\rho_f}{\rho_{nf}} = \frac{1 - \phi + \phi\,(\rho\beta)_p/(\rho\beta)_f}{1 - \phi + \phi\,\rho_p/\rho_f}$$

$$H_3(\phi) = \frac{\lambda_{nf}}{\lambda_f}\frac{(\rho c)_f}{(\rho c)_{nf}} = \frac{1 + 2.944\phi + 19.672\phi^2}{1 - \phi + \phi\,(\rho c)_p/(\rho c)_f}$$

The effective density, specific heat and thermal expansion coefficient of nanofluid are obtained by using the following equations as given by Astanina et al. [5]:

$$\rho_{nf} = (1 - \phi)\rho_f + \phi\rho_p \quad (7)$$

$$(\rho c_p)_{nf} = (1 - \phi)(\rho c_p)_f + \phi(\rho c_p)_p \quad (8)$$

$$(\rho\beta_p)_{nf} = (1 - \phi)(\rho\beta_p)_f + \phi(\rho\beta_p)_p \quad (9)$$

From the experimental data of Ho et al. [6] effective thermal conductivity and effective viscosity can be defined by the following relations:

$$\lambda_{nf} = \lambda_f(1 + 2.944\phi + 19.672\phi^2) \quad (10)$$

$$\mu_{nf} = \mu_f(1 + 4.93\phi + 222.4\phi^2) \quad (11)$$

The above mentioned relations (10) and (11) from [6] of λ_{nf} &μ_{nf} have been obtained by least-square technique for nanofluids varying from ϕ=1%to4% and temperature difference, $T_h - T_c$=2° C to 26° C.

Since only the left vertical wall is heated, local Nusselt number at $\bar{x} = 0$ is calculated by, $Nu_{loc} = -\frac{\lambda_{nf}}{\lambda_f}\frac{\partial\theta}{\partial\bar{x}}$, average Nusselt number in heated walls is obtained by, $\overline{Nu} = \int_0^1 Nu_{loc}\, d\bar{y}$.

III. NUMERICAL METHOD AND VALIDATION

An approximate solution of governing equations (1)-(3) along with boundary conditions (4)-(6) have been obtained by second order scheme based on implicit finite difference method. Error is calculated by, $E = \sum_{i,j=0}^{n} |\xi^{\nu} - \xi^{\nu-1}| / \sum_{i,j=0}^{n} |\xi^{\nu}|$, $\nu = 1,2,3,\ldots$ the calculations are carried out up to $|E| < 10^{-6}$. Here ξ represents the variables $\psi, \omega \; and \; \theta$, ξ^{ν} represents value at ξ for current iteration and $\xi^{\nu-1}$ represents value at previous iteration.

The in house CFD code is verified by comparing the value of Nusselt number(Nu) with previously published papers [4], [7], [8] (Table 1). Also $Fig.1$ shows the streamline and isotheral lines comparison between current work and results of Mohamad et al.[7].

$(a)(b)(c)(d)$

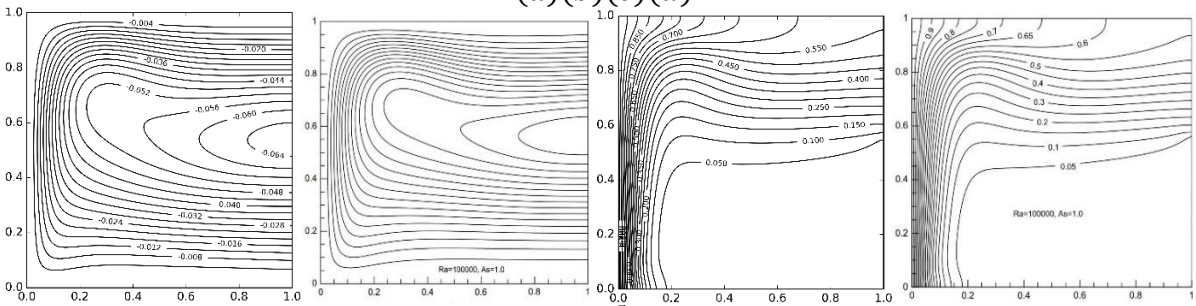

Fig. 2. Comparison of ψ and θ, for $Pr = 0.71$, $Ra = 10^5$, (a) and (c) are obtained in present work for ψ and θ respectably, (b) and (d) are numerical data of Mohamad et al. [7] for ψ and θ respectably.

Outline of the in house CFD code:
Step-1: Initialize ψ, ω and θ.
Step-2: Solve equation (1) for ψ along with the BCs (4)-(6).
Step-3: Solve equation (2) for ω along with the BCs (4)-(6).
Step-4: Solve equation (3) for θ along with the BCs (4)-(6).
Step-5: Calculate error, if conversed go to Step-6 else repeat Step-2 to Step-5.
Step-6: Take the output files, calculate Nusselt number, terminate the program.

Ra	Present work	Miroshnichenko et al. [4]	Mohamad et al. [7]	Mahmoudi et al. [8]
10^4	3.310	3.321	3.377	3.250
10^5	7.333	7.325	7.323	7.237
10^6	14.312	14.322	14.380	14.222

Table 1. Nusselt number comparison ($Pr = 0.71$).

The average Nusselt number variation and CPU time for execution are displayed in Table 1 with $Ra = 10^5, Pr = 6.82, \phi = 0.01, a = 0.5$ and $\gamma = \frac{\pi}{2}$. The computation has been carried out on grid size of 101×101, 201×201, 301×301 and 401×401. Based on the $\overline{Nu}$ variation and time taken by CPU to execute the program, 201×201 grid is considered as most suitable and further computations were made on this grid. The program is executed on an Intel processor with processor base frequency 2.30 GHz (Turbo up to 4.00 GHz). The effect of mesh on vertical velocity component and temperature at $\bar{y} = 0.3$ are shown in $Fig.3$.

Grid size	$\overline{Nu}$	CPU time (in seconds)	$\Delta = \frac{\lvert\overline{Nu}_{201\times201} - \overline{Nu}_{i\times i}\rvert}{\lvert\overline{Nu}_{i\times i}\rvert} \times 100$ %, $(i = 101,301,401)$
101×101	7.548	60.72	0.07%
201×201	7.553	932.91	–
301×301	7.526	4377.88	0.35%
401×401	7.579	12115.06	0.34%

Table 2: Nusselt number comparison for grids of difference size and execution time.

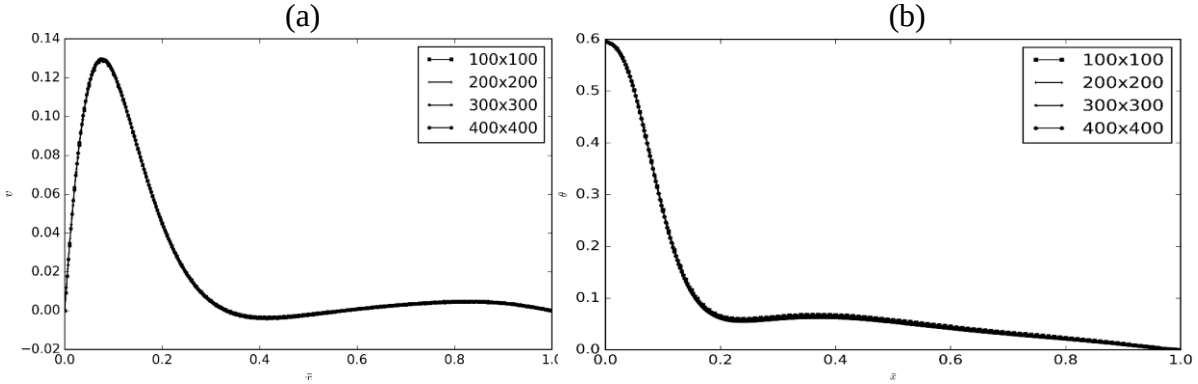

Fig. 3. Effect of mesh on vertical velocity (a) and temperature (b) at $\bar{y} = 0.30$ versus the mesh parameters.

IV. RESULTS AND DISCUSSION

Results of numerical investigation for governing parameters Ra, Pr, ϕ, γ are shown in $Fig.(4) - (8)$. The cold nanofluid enters the cavity through the lower half of open end and then moves towards the heated wall and leaves out through the upper half of theopen end of the cavity. Due to sinusoidal heating, heat generation inside cavity changes significantly.

The contour plots for streamlines and isotherms for $Ra = 10^4$, $Pr = 6.82$ are shown in $Fig.4$ and $Fig.5$ respectively for various values of $\gamma\ (0 - \pi)$ and $\phi(0.00 - 0.04)$. It is observed that flow inside the cavity is affected due to presence of nanofluid and it enhances the convection in the cavity. The value of γ changes heat profile so the position of peak conduction changes, but the flow remains almost symmetric about $\bar{y} = 0.5$, the buoyancy force is not so strong that it can manifest recirculation zones.

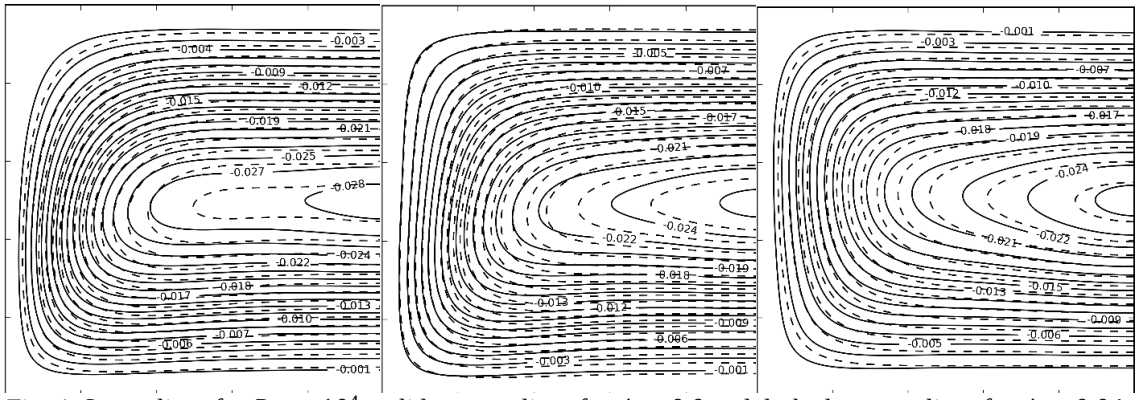

Fig. 4. Streamlines for $Ra = 10^4$; solid contour lines for $\phi = 0.0$ and dashed contour lines for $\phi = 0.04$, left: $\gamma = 0$, middle: $\gamma = \pi/2$, right: $\gamma = \pi$.

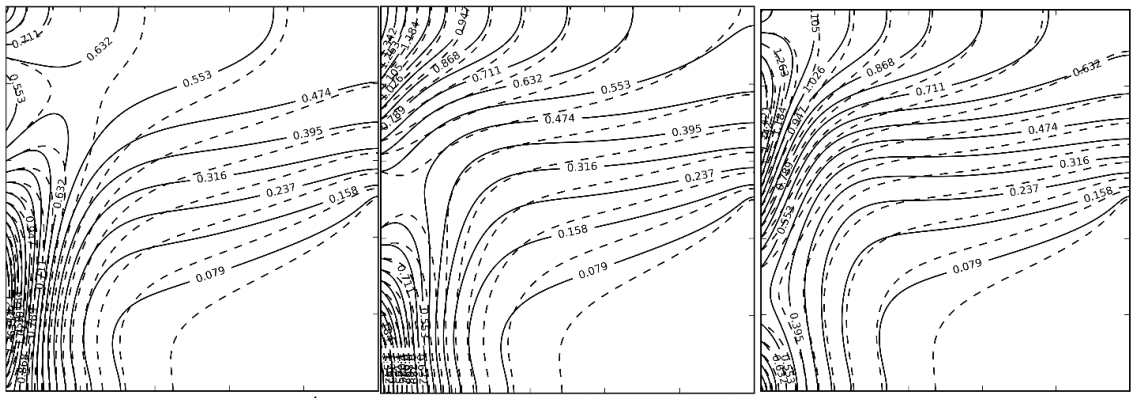

Fig. 5. Isotherms for $Ra = 10^4$; solid contour lines for $\phi = 0.0$ and dashed contour lines for $\phi = 0.04$, left : $\gamma = 0$, middle: $\gamma = \pi/2$, right: $\gamma = \pi$.

For $Ra = 10^5$, $Pr = 6.82$, the contour plots of streamlines and isotherms are shown in $Fig.6$ and $Fig.7$ respectively for various values of γ $(0 - \pi)$ and $\phi(0.00 - 0.04)$. From these figures, it is observed that heat propagation is negligible in the presence of nanoparticles. The flow pattern is analogous to flow pattern obtained for $Ra = 10^4$. As Ra increases the heat propagation in horizontal direction reduces and convective recirculation generates close to heated wall. The effect of buoyancy is more prominent in the presence of nanoparticles so that recirculation gets formed.

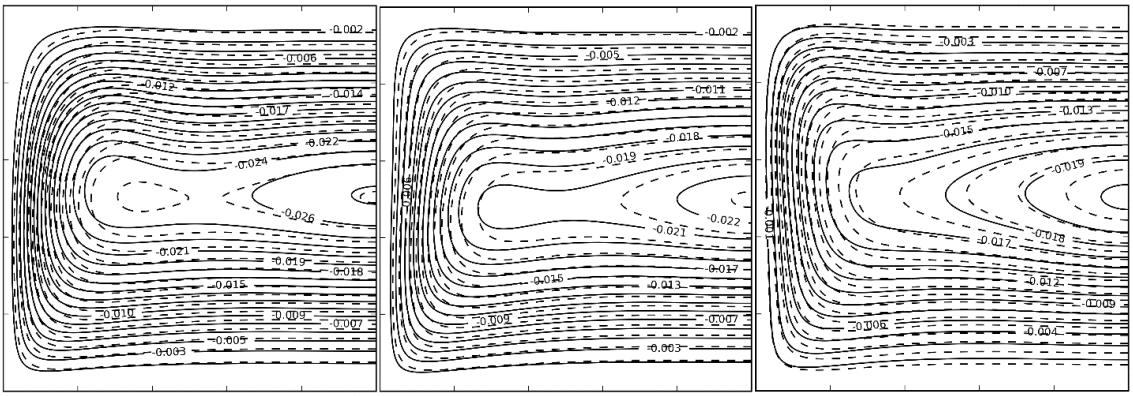

Fig. 6. Streamlines for $Ra = 10^5$; solid contour lines for $\phi = 0.0$ and dashed contour lines for $\phi = 0.04$, left: $\gamma = 0$, middle: $\gamma = \pi/2$, right: $\gamma = \pi$.

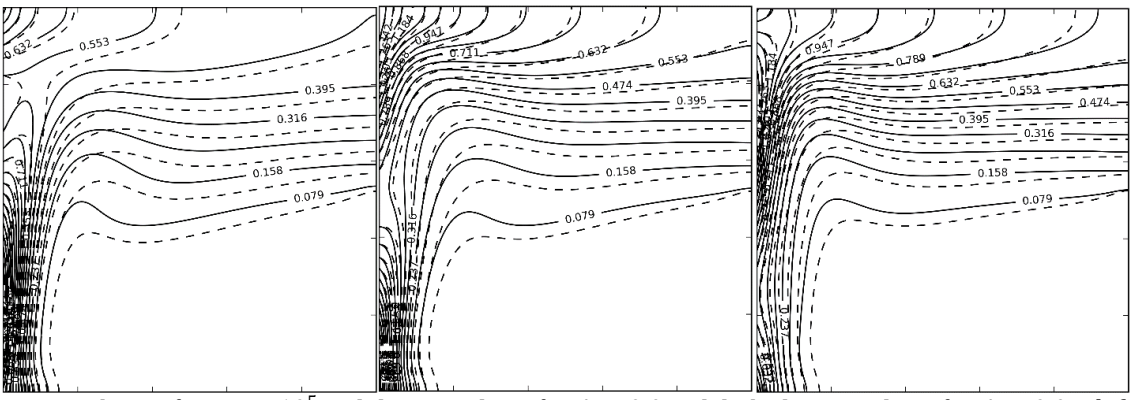

Fig. 7. Isotherms for $Ra = 10^5$; solid contour lines for $\phi = 0.0$ and dashed contour lines for $\phi = 0.04$, left : $\gamma = 0$, middle: $\gamma = \pi/2$, right: $\gamma = \pi$.

It is expected that the variation ofNu value with sinusoidal heat profile is different as compared to uniformly heat conducting wall. When heat transfer is natural environment to the cavity, Nu become positive and in case heat flows out of cavity through low temperature portions of heated wall, Nu values becomes negative. From $Fig.8$, it is clear that conduction is more prominent for $Ra = 10^5$ as compared to $Ra = 10^4$, also depending on values of γ the heating profile changes as a result the position of peak conduction also changes, at $\gamma = 0$ maximum conduction takes place at the lower portion of the cavity and at $\gamma = \pi$ the position of maximum conduction moves upwards of the heated wall.

The average Nusselt number $(\overline{Nu})$ is calculated along the heated wall and presented in Table 3. The values are presented for different values of Ra and γ, $\overline{Nu}$ value under the presence of nano particle are presented inside parenthesis. It is observed that presence of nanoparticle reduces overall convection along the active wall and increment of Ra enhances convection to the conduction whereas for all Ra value maximum convection takes place when $\gamma = \pi$. Using least square technique the correlations are obtained for,$Ra = 10^4$ and $\phi = 0.04$, $\overline{Nu} = 2.831 - 0.314\gamma + 0.135\gamma^2$when$0 \le \gamma \le \pi$ and for $Ra = 10^5, \phi = 0.04, \overline{Nu} = 7.387 - 0.60729888\gamma + 0.24988699\gamma^2$, here $0 \le \gamma \le \pi$.

Ra	$\gamma = 0$	$\gamma = \pi/4$	$\gamma = \pi/2$	$\gamma = 3\pi/2$	$\gamma = \pi$
10^4	3.358(2.843)	3.110(2.648)	3.096(2.656)	3.323(2.883)	3.658(3.163)
10^5	7.883(7.396)	7.584(7.055)	7.630(7.024)	7.983(7.387)	8.475(7.928)

Table 3: Average Nusselt number for different γ value, values inside parenthesis are for nanofluid.

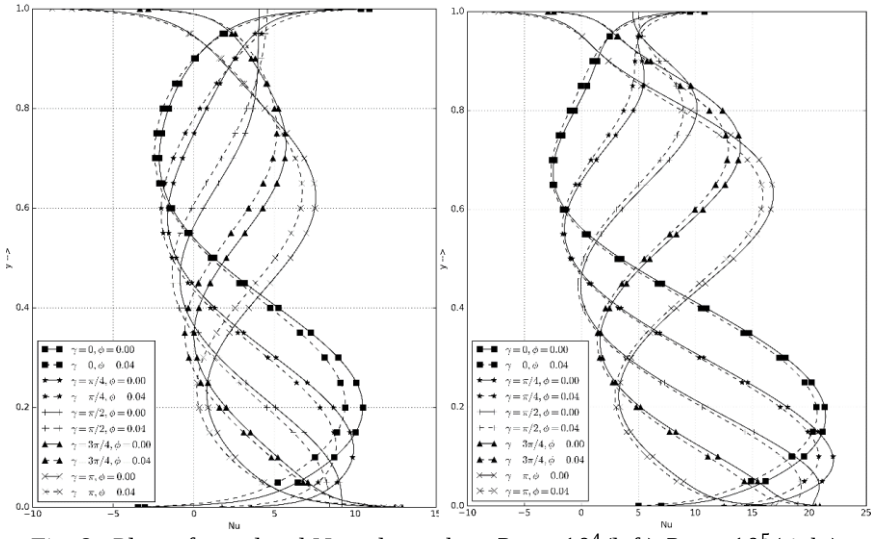

Fig. 8. Plots of $\bar{y}$ vs local Nusselt number, $Ra = 10^4$(left),$Ra = 10^5$(right).

V. CONCLUSIONS

From the results obtained by the investigation the following conclusion are drawn:

- The presence of nanofluid influences the thermal propagation at low Ra value, as Ra increases the effect of nanofluid decreases.
- Sinusoidal heating profile having the phase $\gamma\,(0-\pi)$ the flow inside the cavity remains almost symmetrical with respect to $\bar{y} = 0.5$.
- The local Nusselt may become negative and positive as well. The negative Nusselt number indicates the heat is transferred to natural environment from enclosure. Whereas positive Nusselt number indicates that the heat is transformed inside the cavity from heated wall. The local Nusselt number on the active wall depends on γ.

ACKNOWLEDGEMENTS

The first author wishes to express thank IIT(ISM), Dhanbad for financial support.

REFERENCE

[1]. S. Ostrach, "Natural Convection in Enclosures," vol. 8, J. P. Hartnett and T. F. Irvine, Eds., Elsevier, 1972, pp. 161-227.
[2]. E. Bilgen and R. B. Yedder, "Natural convection in enclosure with heating and cooling by sinusoidal temperature profiles on one side," International Journal of Heat and Mass Transfer, vol. 50, pp. 139-150, 2007.
[3]. H. F. Öztop, P. Estellé, W.-M. Yan, K. Al-Salem, J. Orfi and O. Mahian, "A brief review of natural convection in enclosures under localized heating with and without nanofluids," International Communications in Heat and Mass Transfer, vol. 60, pp. 37-44, 2015.
[4]. I. V. Miroshnichenko, M. A. Sheremet, H. F. Oztop and N. Abu-Hamdeh, "Natural convection of alumina-water nanofluid in an open cavity having multiple porous layers," International Journal of Heat and Mass Transfer, vol. 125, pp. 648-657, 2018.
[5]. M. S. Astanina, M. A. Sheremet, H. F. Oztop and N. Abu-Hamdeh, "Mixed convection of Al2O3-water nanofluid in a lid-driven cavity having two porous layers," International Journal of Heat and Mass Transfer, vol. 118, pp. 527-537, 2018.
[6]. C. J. Ho, W. K. Liu, Y. S. Chang and C. C. Lin, "Natural convection heat transfer of alumina-water nanofluid in vertical square enclosures: An experimental study," International Journal of Thermal Sciences, vol. 49, pp. 1345-1353, 2010.
[7]. A. A. Mohamad, M. El-Ganaoui and R. Bennacer, "Lattice Boltzmann simulation of natural convection in an open ended cavity," International Journal of Thermal Sciences, vol. 48, pp. 1870-1875, 2009.
[8]. A. Mahmoudi, I. Mejri, M. A. Abbassi and A. Omri, "Analysis of MHD natural convection in a nanofluid-filled open cavity with non uniform boundary condition in the presence of uniform heat generation/absorption," Powder Technology, vol. 269, pp. 275-289, 2015.

Nomenclature:

Roman letters and Greek symbols:

a	amplitude of sinusoidal heating	c	specific heat
H_1, H_2, H_3	special functions	L	length and height of cavity
Nu	local Nusselt number	$\overline{Nu}$	average Nusselt number
Pr	Prandtl number	Ra	Rayleigh number
T	dimensional time	T_c	cold wall temperature
T_h	hot wall temperature	u, v	dimensional velocity components
$\bar{u}, \bar{v}$	dimensionless velocity components	x, y	dimensional coordinates
$\bar{x}, \bar{y}$	dimensionless coordinates	θ	dimensionless temperature
λ	thermal conductivity	ρ	density
ρc	heat capacitance	$\rho\beta$	buoyancy coefficient
ϕ	nanoparticles volume fraction	ψ	dimensionless stream function
ω	dimensionless vorticity	BC	boundary condition

Subscripts:

c	cold	f	fluid
h	hot	nf	nanofluid
p	(nano) particle		